UNIVERSITÀ DI PARMA
ARCHIVIO DELLA RICERCA

University of Parma Research Repository

Petrophysical properties of deformation bands in high porous sandstones across fault zones in the Rio do Peixe Basin, Brazil

This is the peer reviewd version of the followng article:

Original
Petrophysical properties of deformation bands in high porous sandstones across fault zones in the Rio do Peixe Basin, Brazil / Pontes, C. C. C.; Nogueira, F. C. C.; Bezerra, F. H. R.; Balsamo, F.; Miranda, T. S.; Nicchio, M. A.; Souza, J. A. B.; Carvalho, B. R. B. M.. - In: INTERNATIONAL JOURNAL OF ROCK MECHANICS AND MINING SCIENCES. - ISSN 1365-1609. - 114:(2019), pp. 153-163. [10.1016/j.ijrmms.2018.12.009]

Availability:
This version is available at: 11381/2865709 since: 2019-10-30T13:13:37Z

Publisher:
Elsevier Ltd

Published
DOI:10.1016/j.ijrmms.2018.12.009

Terms of use:

Anyone can freely access the full text of works made available as "Open Access". Works made available

Publisher copyright

note finali coverpage

(Article begins on next page)

24 April 2024

International Journal of Rock Mechanics and Mining Sciences xxx (2018) xxx-xxx

Contents lists available at ScienceDirect

International Journal of Rock Mechanics and Mining Sciences

journal homepage: www.elsevier.com

Petrophysical properties of deformation bands in high porous sandstones across fault zones in the Rio do Peixe Basin, Brazil

Cayo César Cortez Pontes[a], Francisco Cézar Costa Nogueira[b], Francisco Hilário Rêgo Bezerra[a], Fabrizio Balsamo[c], Tiago Siqueira de Miranda[d], Matheus Amador Nicchio[c], Jorge André Braz de Souza[e], Bruno Raphael Barbosa Melo de Carvalho[e]

[a] *Universidade Federal do Rio Grande do Norte, Rua dos Perdizes - Pitimbu, 59064-480. Nata, Rio Grande do Norte, Brazil*
[b] *Universidade Federal de Campina Grande, Brazil*
[c] *Dipartimento di Scienze della Terra, Università degli Studi di Parma, Parco Area delle Scienze 157A, 43100 Parma, Italy*
[d] *Universidade Federal de Pernambuco, Brazil*
[e] *CENPES/Petrobras S.A, Brazil*

ARTICLE INFO

Keywords:
Deformation bands
Uniaxial compressive strength
Petrophysics properties

ABSTRACT

In this contribution we show the variation of the uniaxial compressive strength (UCS) and petrophysical properties of different architectural elements of fault zones affecting poorly lithified coarse sandstone and conglomerates of the Rio do Peixe basin, NE Brazil. We worked on three distinct outcrops; (1) non-deformed (protolith); (2) single fault zone, presenting moderate strain; and (3) complex fault zone, presenting a high strain intensity, were multiple and well developed fault cores occurs. To characterize the structural domains, we performed scanlines and uniaxial geomechanical survey across deformation bands and clustering zones. We combined geomechanical data with porosity data acquired thru image analysis and gas expansion analysis. We acquired data on deformation band cores and zones between deformation bands (*i.e.,* deformed zones that do not present deformation bands). Our results shows that the complex fault zone exhibits a strong increasing on the rock resistance. Thus presenting UCS values three times higher than the obtained on the single fault zone outcrop and four times higher when compared with the non-deformed outcrop. It suggests that there is a direct relation between strain and rock resistance. The porosity is also strongly affected by the deformation, exhibiting an inverse relation with the strain intensity. Complex fault zone presents up to 75% of porosity reduction, while single fault zone, only about 10% of reduction. The petrophysical properties were calculated in the complex fault zone, where the resistance of the DBs was as high as twice that of the zone without bands, which had effects on the Young's and the incompressibility's moduli. The results suggest that even though DBs generate up to a 40% increase in the UCS and a 75% decrease in the porosity, the structural domains where the rock is located strongly controls the geomechanical and petrophysical properties. Thus, directly affecting the anisotropy of a reservoir.

1. Introduction

Deformation bands (DBs)[1] are tabular structures that occur in porous rocks and are characterized by volumetric changes caused by different deformation mechanisms, such as cataclasis or granular flow, and kinematics with shear offset (>10 mm).[2–5] These structures were initially described by Aydin[1] as small faults measuring several millimetres in thickness and a few meter in length. DBs have characteristic processes, such as pore collapse and grain fracturing, and can be effective hydrocarbon seals even with small offsets.[6–8]

DBs can act as either hydraulic barriers or conduits for fluid flow, depending on the mechanisms of deformation and factors, such as confining pressure occurring during their formation and structural evolution.[4,9–14] These hydraulic behaviours stimulated investigations into their geomechanical, petrophysical and fault distribution properties to predict the modalities of fluid flow during the development and depletion of oil reservoirs.[15–17] Obtaining extensive and detailed knowledge

Email addresses: cayopontes@ufrn.edu.br (C.C.C. Pontes); francisco.nogueira@ufcg.edu.br (F.C.C. Nogueira); bezerrafh@geologia.ufrn.br (F.H.R. Bezerra); fabrizio.balsamo@unipr.it (F. Balsamo); tiago.smiranda@ufpe.br (T.S. de Miranda); matheus.amadornicchio@unipr.it (M.A. Nicchio); jorgeabs@petrobras.com.br (J.A.B. de Souza); brcarvalho@petrobras.com.br (B.R.B.M. de Carvalho)

https://doi.org/10.1016/j.ijrmms.2018.12.009
Received 24 May 2017; Received in revised form 22 November 2018; Accepted 6 December 2018
Available online xxx
1365-1609/ © 2018.

UNCORRECTED PROOF

of these flow properties has fundamental importance in the analysis of the fluid migration pattern and the rock storage properties.[18,19]

DBs directly affect the petrophysical properties of sandstones, such porosity and permeability[20] as well as the geomechanical properties such as UCS and Young's modulus.[21] These structures can act in different ways in the reservoir. The cataclastic bands, which have mechanical fracture of the grains as the main mechanism, usually present reduction of permeability and porosity in relation to the host rock, while UCS and Young's modulus tend to increase relative to their host rock.[13] On the other hand, disaggregation bands, which form by granular flow as the main mechanism, tend to present an increase of porosity and a decrease in UCS and Yong's modulus.[22]

An analysis of different structural domains within the fault zone, such as the fault core and damage zone,[23–25] combined with geological, geomechanical and petrophysical analyses are fundamental to the understanding of the compartmentalization of oil reservoirs. The density and the geomechanical characteristics and petrophysical properties of DBs are parameters closely related to each other, which directly influence the behavior of the reservoir.[3,16,26] The comprehension of the variation of properties as UCS, porosity, the Young's and incompressibility moduli and the Poisson's ratio are essential in the study of reservoirs.

Several studies have presented the structure and evolution of fault zones in sedimentary deposits, their influence on fluid flow, and how these structures and evolution define different structural domains.[4,6,14,17,25,27,28] However, the study of the geomechanical and petrophysical properties of DBs across fault zones, in different deformational domains (Fig. 1) or in the same domain, is still poorly investigated.

The aim of the present study is to show the role of different structural domains in changes in the physical properties of porous rocks within deformation band fault zones, identify the changes on porosity, Young's modulus, incompressibility modulus, Poisson's ratio and UCS. The study area is located in the Rio do Peixe Basin (RPB) in northeastern Brazil (Fig. 2A). The petrophysical properties are addressed in different architectural components of a regional scale fault zone: (1) high strain zone with multiple cores, (2) moderate strain zone with single core, and (3) protolith (Fig. 2B) in siliciclastic units. The specific aim of this study is to analyse the relationship between the frequency of DBs, fault zone architectures and petrophysical properties.

2. Geological settings

The Rio do Peixe Basin is a sedimentary basin formed during the rifting and breakup of the African and South American continents from the Neocomian to the Barremian.[29,30] The basin is composed of three sub-basins, representing three half-grabens named, from west to east, the Brejo das Feiras, Sousa and Pombal sub-basins[29,31] (Fig. 1B), separated by basement horsts. The main shear zones that bind the Rio do Peixe Basin are the Portalegre, Malta and Rio Piranhas[29] (Fig. 1B).

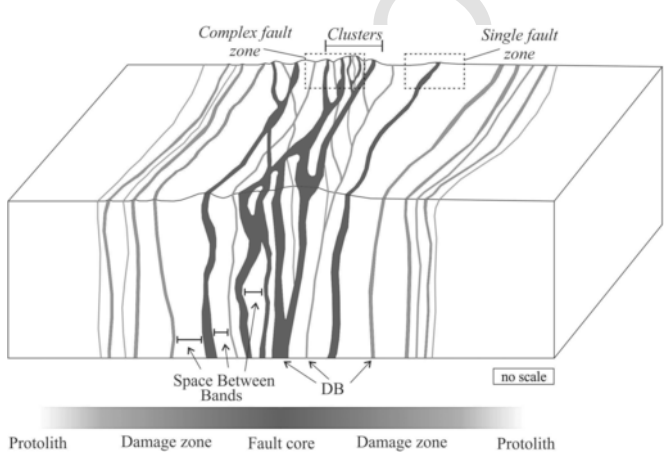

Fig. 1. (A) Schematic model of petrophysical properties across a fault zone (modified from Faulkner et al., 2010; Choi et al., 2016). The width of DBs are exaggerated for the sake of clarity.

The evolution of these sub-basins was related to the brittle reactivation of the Precambrian ductile shear zones. DBs in this basin were first described by Sénant and Popoff,[31] and their kinematics and geological features were presented by Nogueira et al.,[30] whereas Nicchio et al.[32] and Araujo et al.[33] described the cataclastic DBs in the basin.

The sedimentary infill of the Rio do Peixe Basin consists of three different formations of the Early Cretaceous age[31]: Antenor Navarro, Sousa and Rio Piranhas, respectively.[34] The Antenor Navarro Formation directly overlies the crystalline basement, as an unconformity that occurs along the flexural margins of the half-grabens.[31] The Antenor Navarro Formation is composed of conglomerates and immature sandstones at the base, and fine sandstones interfingered with shales at the top. The Sousa Formation is the intermediate unit, which is composed of shales and reddish silts deposited in a lacustrine system. The Rio Piranhas Formation is composed of conglomerates and coarse sandstones deposited in alluvial fan systems.[35]

3. Methods

3.1. Field investigation

This study was performed on conglomerate sandstone with a fine to clay matrix from the Antenor Navarro Formation affected by cataclastic DBs (Fig. 3A). The analysis of the different structural domains and host rocks were performed using field and laboratory procedures. The fieldwork included *in situ* geomechanical profiles with an L-type Schmidt Hammer, structural attributes analysis collected along continuous scanlines oriented to intercept the highest number of structures, following procedures presented by.[36–40] The different fault zones were sampled for petrographic and petrophysical analyses.

We performed Schmidt hammer tests following the procedures outlined by Aydin,[41] such as the calibration of the apparatus before analysis. The sampling was performed perpendicularly to the outcrop surface. The laboratory analysis consisted of measuring the porosity and dynamic properties, Young's modulus, incompressibility modulus, and the Poisson Ratio. However, the plug sampling was possible only in the fault core, where the rock presents a high degree of cohesion. The porosity values were obtained through two methods: thin section image and plugs analysis. In the thin sections, we observed different intensities of deformation such as a high cataclastic zone (HCZ) and the porosity was calculated with processed (binarized) thin section images (Fig. 3B) using the Avizo Fire software®. The porosity measurement was also performed in cylindrical rock samples (3.5–5.0 cm long and 3.0 cm in diameter) using the method of gas expansion. We used the UltraPoroPerm500 equipment to perform the porosimetry measurements, from which we obtained the Young's and incompressibility moduli and the Poisson's ratio using wave velocity relationships. The compressional and shear wave velocities were obtained using the AutoLab500 equipment.

We analysed three outcrops that represent different strain intensities. Outcrop 1 corresponds to the non-deformed protolith (Fig. 4A), with undeformed sedimentary structures. Outcrop 2 presents a moderate strain intensity, exhibiting one single meter-thick fault core and is characterized by a low number of DBs, a moderate degree of deformation, only one DB cluster, moderate cohesion, and no slip surfaces (Fig. 4B). Outcrop 3 is intensely deformed, were several well developed fault cores occurs, thus forming a complex fault zone expressed by a great number of DBs, slip surfaces and high cohesion sandstone (Fig. 4C). These last two outcrops present DBs as the main structures, either as

CORRECTED PROOF

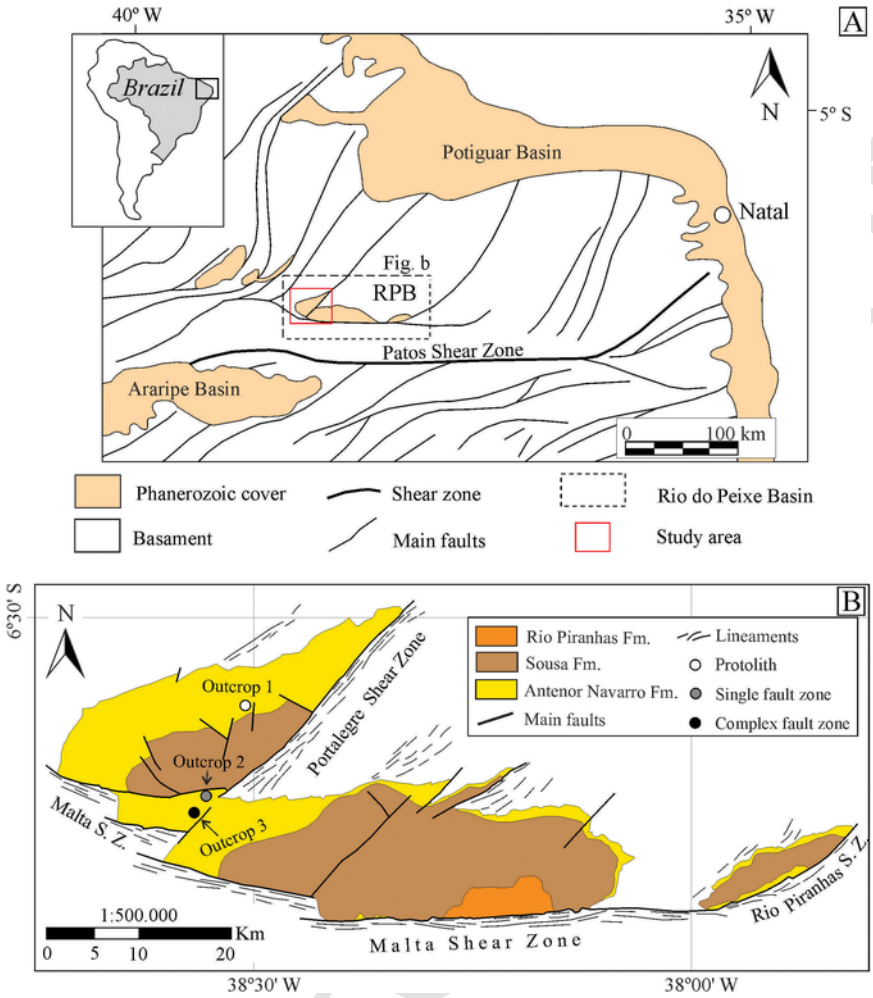

Fig. 2. (A) Location of the Rio do Peixe Basin; (B) Simplified geological map of the basin (modified from Françolin et al., 1994 and Medeiros et al., 2005) with the localization of the outcrops representing the protolith (outcrop 1), single fault zone (outcrop 2) and complex fault zone (outcrop 3).

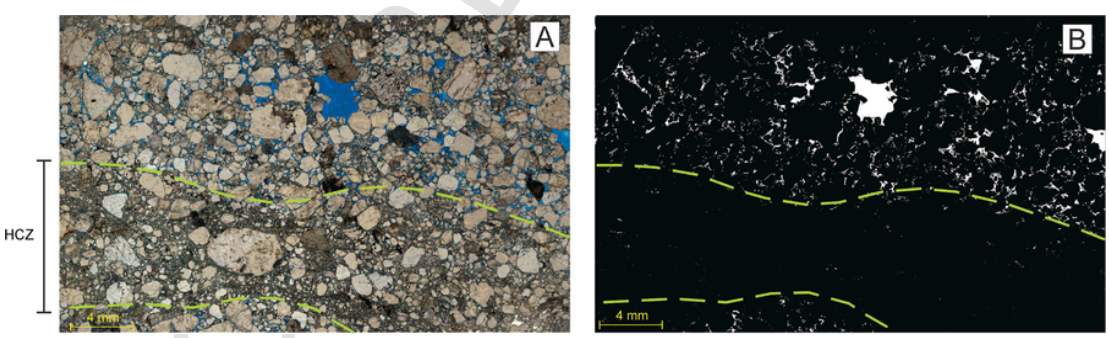

Fig. 3. (A) Photomosaic of a thin section with cataclastic shear bands, presenting a high cataclastic zone (HCZ) and a (B) processed image (binarized) of the same thin section.

isolated structures (singles) or as complex zones of multiple structures (clusters).[4,42]

3.2. Geomechanical analysis

Geomechanical profiles were conducted in the three outcrops using an L-type Schmidt Hammer to detect rebound value variations among the three structural domains. In damage zone and fault core areas, the analyses were performed punctually on the DBs and at the points between the deformation bands (Fig. 4D). Measuring the values inside and between the DBs was important to understand their effect on the UCS between and the UCS variations inside the same structural domain. The direction and length of the profiles were defined to intercept the largest possible number of structures both in single and in cluster zones, covering the whole outcrop. The methodology adopted to collect the geomechanical data followed the standards of the American Society for Testing and Materials[43] in which 10 measurements of rebound values were performed for each point and an average of these was calculated. Finally, the UCS values were compared with a compilation of UCS values in medium/coarse sandstones presented by Baud et al.[44].

The measurement of the UCS values were the following: 21 measurements in the protolith (outcrop 1); 62 measurements in single fault zone (outcrop 2), 35 of which were in the DBs and the 27 in the host rock between these bands; 36 measurements in the complex fault zone

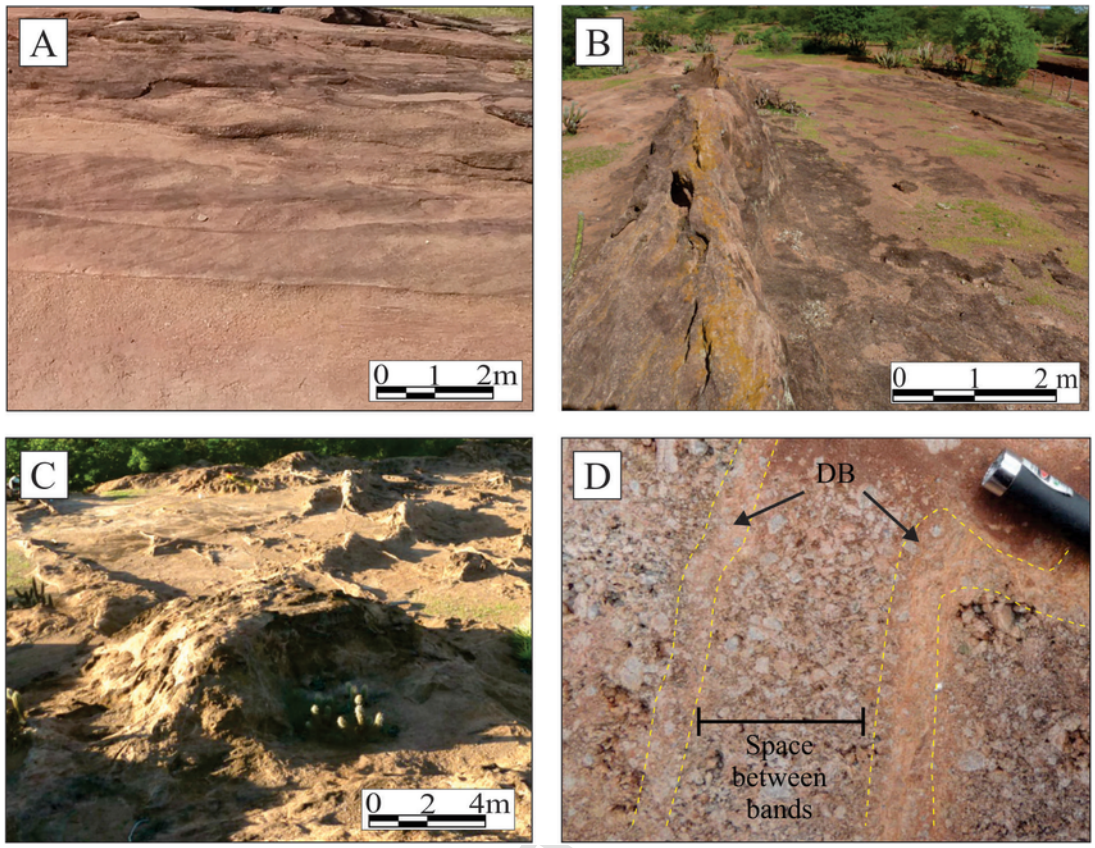

Fig. 4. (A) Outcrop from protolith; (B) Single fault zone; (C) Complex fault zone, with great number of clusters; and (D) Variation between DBs zone and spacing between bands present in the same structural domain.

(outcrop 3), 15 of which correspond to values obtained in the DB and the other 21 in zones between bands.

3.3. Scanline

Outcrops were selected for measuring DB's attributes in the different architectural elements: protolith, single fault zone and complex fault zone (Table 1). We performed four scanline surveys orthogonal to the DB strikes following the rationale described by.[38,45,46] The measurements in the scanlines that were not exactly perpendicular to the sets of DBs were corrected using corrections after Terzaghi.[47] The following features were measured along the scanlines: a) spacing (perpendicular distance) between bands; b) band thickness; c) band strike; d) abutting relations; and f) the composition of the band.[37,38,48–50] On the outcrop, the thickness of the DBs were measured using a hand lens and a comparator,[38] which allowed measurement to approximately 0.05 mm by comparing the fracture width with a printed stripe of precisely determined thickness.[49]

Two scanlines were performed in the single fault zone (outcrop 2), SC-1 and SC-2, both striking NS, and 28 m and 6 m long, respectively (Fig. 5A). We performed two scanlines in the complex fault zone: SC-3, SC-4 *ca.* with a combined length of 40 m (Fig. 5B). These surveys were performed perpendicular to the sets of DBs identified in the outcrop and they strike NW-SE. The regularity of the spacing of the DBs in the single and complex fault zones was quantified by the coefficient of variation (CV) of the population of the spacing between the bands.

$$CV = \sigma / \mu \quad (1)$$

where σ is the standard deviation of the spacing population, and μ is the arithmetic mean. For a random distribution of DBs $CV = 1$. Then, if $CV > 1$, the DBs are more clustered than random; when $CV < 1$, the distribution of the DBs presents as less clustered, and there is a greater regularity in the spatial organization of these bands.[49,51]

Table 1
Scanline descriptions. AE = architectural elements; SFZ = single fault zone; CFZ = Complex Fault Zone.

Scanline	AE	Scanlinedirection	Scanline length (m)	Number of DB's	CV spacing (-)
SC-1	SFZ	N-S	28	41	1.86
SC-2	SFZ	N-S	6	21	2.1
SC-3	CFZ	NW-SE	20	117	1.0
SC-4	CFZ	NW-SE	19	114	5.0

3.4. Petrophysical analysis

Rock samples were collected in the outcrops of the three fault structural domains to estimate the porosity. However, sampling plugs was only possible in the complex fault zone, where the rock presents a high degree of cohesion. The determination of porosity in all the structural domains was performed in thin sections. The thin sections were made with the DBs in the centre of the section to capture textural and porosity variations inside and outside the bands. Then, the entire thin sections were imaged, and these images were processed in the Avizo Fire® software to identify pores and grains and then calculate the porosity. The petrophysical properties determination in the plugs used a different method. Initially, the plugs were sawn to the length of *ca.* 6.3 cm, with a diameter of 3.8 cm. The extremities were smoothed to a perfect cylinder, and, before starting the analysis, the sample was subjected to 24 h at 80 ºC in a greenhouse. The petrophysical analysis in the plugs was performed in a permoporosimeter by gas expansion, using an Ul-

UNCORRECTED

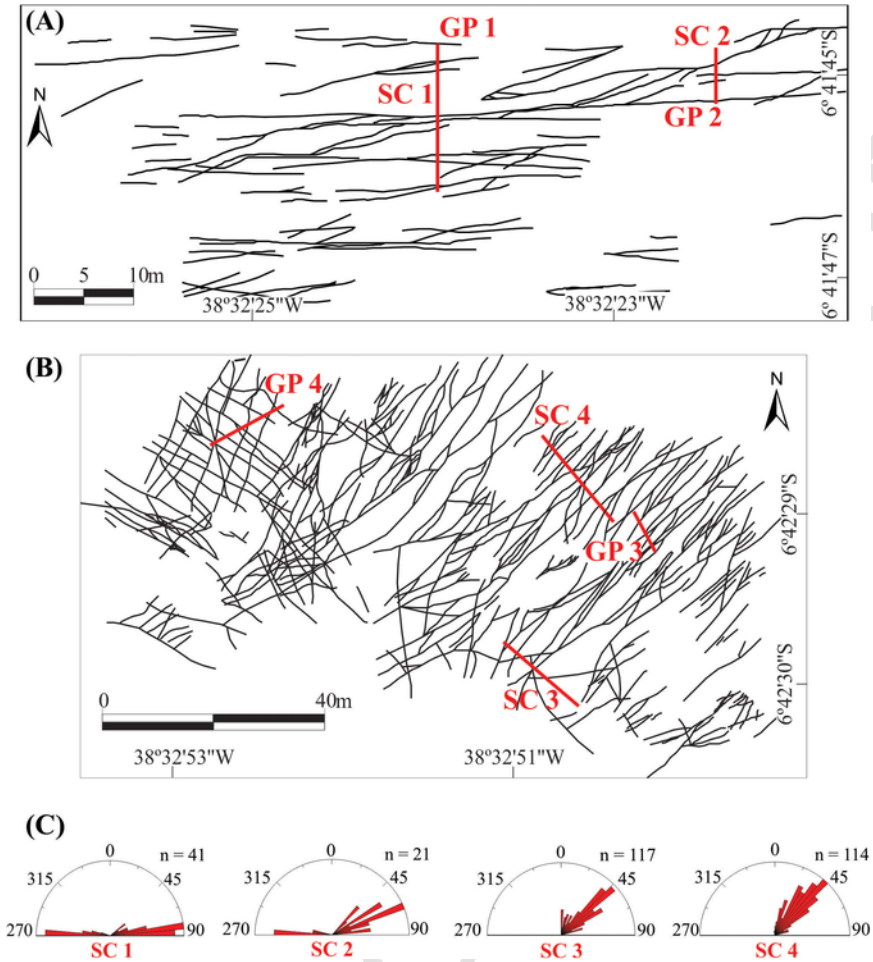

Fig. 5. (A) Position of geomechanical profile (GP) and scanlines (SC) conducted in the single fault zone and (B) complex fault zone. (C) Rose diagrams of the strikes of DBs. Key: n = number of bands. Location of the outcrops in Fig. 2B.

traPoroPerm 500. The Young's and incompressibility moduli and Poisson's Ratio were derived through empirical relations of wave velocity using the AutoLab500 apparatus.

4. Results

4.1. General characteristics of fault zone domains

The structural domains were identified in the field: (1) the protolith (Fig. 4A); (2) the single fault zone (Fig. 4B); and (3) the complex fault zone (Fig. 4C). The protolith consists of non-deformed rock, thus presenting no DBs and preserving its original sedimentary structure, such as cross stratification. Another specific characteristic is the low cohesion. The single fault zone is characterized by a relatively moderately strain, where an isolated deformation band clustering zone occurs as the main fault core and is marked by bands with an average spacing of 20 cm and forming a few clusters (Fig. 3B). The DBs strike NE and EW (Fig. 5C). The complex fault zone present several fault zones, exhibiting well-developed meter-thick deformation band clustering zones. The complex fault zone (Fig. 4C) is intensely deformed, exhibiting a greater number of NE-, NW-, EW- and NS-striking DBs (Fig. 5C). The fault zone is marked by several clusters that exhibit positive topographic relief, thus marking a greater resistance to weathering. It is important to note that the outcrops present no geological markers for a precisely measurement of fault offset. However, if we apply empirical methods such as the length-displacement relation,[52] we could infer a displacement of less than 1 m for the single fault zone and between 1 and 1,5 m displacement for each individual fault zone present in the complex fault zone outcrop.

4.2. Uniaxial Compressive Strength (UCS)

The distributions of the estimated values of the UCS in the different architectural elements of the fault zone are shown in Fig. 6. The profiles were conducted to acquire data across the fault zone. In the undeformed rock, which presents low cohesion, the lowest UCS among all the elements that make up the fault zone values were recorded, varying from 6.5 to 12 MPa, with an average value of 10 MPa (Fig. 6).

In the single fault zone, the UCS values vary between 6.5 and 38.0 MPa with an average value of 16.3 MPa. In the zone between DBs, the values vary between 6.0 and 25.0 MPa with an average value of 11.4 MPa (Fig. 6). Each architectural element has two different values of UCS for analysis in the DBs and between DBs. The values measured in the DB have greater values than those between the DBs (Fig. 6). Such behavior is observed both in single and complex fault zones, where the points with DBs present higher resistance values than those zones between the DBs.

However, when the UCS values for the three structural domains are compared, the geomechanical profiles conducted in the single fault zone, even with the presence of the DBs, presented a lower resistance value when compared to the complex fault zone (Fig. 6). In the complex fault zone, the resistance values obtained within the deformed zones with the DBs vary between 44 and 59 MPa with an average value of 52.4 MPa, whereas the measurements made in the zones between

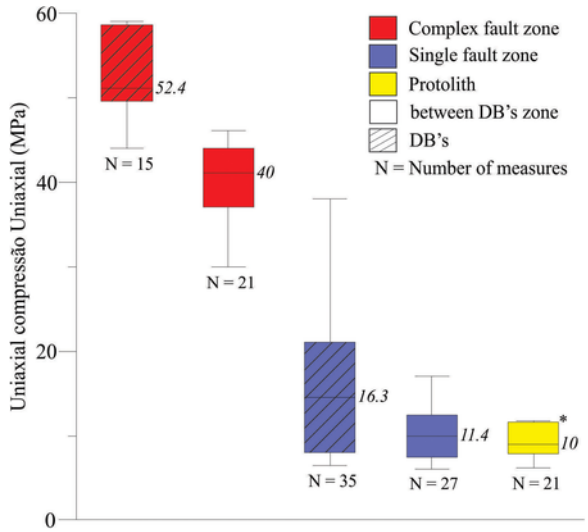

Fig. 6. Uniaxial compressive strength values in each of the architectural elements of the fault zone. * have no DBs.

the bands vary between 30 and 45 MPa with an average of 40 MPa (Fig. 6). Therefore, the resistance values in the DBs are 25% higher than in the sites between the DBs.

4.3. Scanlines

DBs strike in the four directions: a) NE-SW; b) EW; c) NW-SE and d) NS. Scanline SC-1, 28 m long, crossed 41 DBs that strike EW. The coefficient of variation (*CV*) of 1.86 indicates irregular spacing between the bands in the single fault zone (Table 1). The thickness distribution has a linear trend and is consistent with a power law distribution (Fig. 7A) with a high coefficient of determination of $R^2 = 0.97$.

Scanline SC-02 cut across 21 DBs along 6 m and has a *CV* of 2.1, indicating spacing that is more clustered than random in the damage zone. The thickness distribution fit with a power-law function with an exponent of - 0.80 and a coefficient of determination $R^2 = 0.91$ (Fig. 7B).

Scanline SC-3 intercepts 117 NE-SW-striking DBs along 20 m in the core fault region (Fig. 7C). The processing of scanline data allowed us to describe the thickness-size distribution in the log-log plot (cumulative frequency *versus* kinematic aperture), which fit a power-law equation having a scaling exponent of about - 0.89 and a *CV* value of 1.0 (randomly spaced).

Scanline SC-4 is 19 m long, cut across 114 NE-SW-striking DBs and has a CV value of 5.0, indicating a great clustering tendency in the fault core. The thickness distribution fit a power-law function with a - 0.78 exponent and a coefficient of determination $R^2 = 0.94$ (Fig. 7D).

The complex fault zone has a frequency of bands/m up to four times greater than that of the single fault zone. These results agree with a *CV* of 5.0 in the complex fault zone core and 1.86 in the single fault zone (Table 1). Furthermore, the average values of thicker bands range from 5.0 to 7.5 mm in the fault core and 1.9–4.6 mm in the single fault zone. Moreover, the complex fault zone has a band spacing 2.5 times smaller than that in the single fault zone, where the significantly larger presence of clustered bands in the more deformed portion directly influences this increase of frequency in this zone.

4.4. Porosity measured in thin section

The porosity values measured on the thin sections (Table 2) show higher porosity in the region of the non-deformed protolith followed by the single fault and finally the complex fault zone, which had the lowest values of porosity.

The protolith, with an average porosity of 10.3%, exhibits large porosity (Fig. 8 A, B) and the predominance of punctual contacts between the grains. These protolith features indicate a low degree of compaction. The single fault zone exhibits a reduction in porosity and moderate compaction, with 8.9% of average porosity (Fig. 8 C, D). The contacts between the grains are punctual or long, with formation of fractures by compaction along grain contacts.

An intense reduction of the porosity occurs in the complex fault zone (Fig. 8E, F). The contacts between the grains are predominantly long and sometimes sutured, indicating a high degree of compaction. The grain fracturing varies from moderate to intense, generating a cataclastic matrix that fills the remaining pores. The average porosity value in the fault core is 2.5%, which indicates a reduction of more than 75% in porosity when compared to the protolith.

4.5. Porosity determination by gas expansion and dynamic properties

Only the complex fault zone presented enough cohesion for the removal of the plugs, allowing both conventional porosity analysis and the calculation of Young's modulus, incompressibility and Poisson's ratio by empirical relations using wave velocity. The results were divided into samples with and without DBs. However, it is important to emphasize that the samples with DBs are very anisotropic when compared to samples without DBs. The average value of porosity for samples containing DBs by the conventional method is 13.2%, whereas for samples with no band this value is 19.8% (Fig. 9A). The presence of the DBs in this case results in a porosity reduction greater than 30%.

The Young's modulus values for the samples with no DB varied between 15 and 27 GPa, whereas for the units with DBs, those values range from 31 to 47 GPa (Fig. 9B). In addition, the higher the Young's modulus, the smaller the porosity values. Thus, the samples with smaller Young's modulus are those with less resistance to deformation. These values in laboratory analysis corroborate with the UCS values obtained in the field, where the DBs present higher values of resistance (Fig. 6). Higher Young's modulus and UCS values can be attributed to the analysed DBs, which may possibly have led to an increase in the cohesion of the sandstones and conglomerates.

Higher incompressibility values resulted in greater resistance to triaxial deformation in these units because of the hydrostatic deformation. The incompressibility modulus (Fig. 9C) shows values between 8 and 15 GPa for the samples between DBs, while rocks with DBs have values between 16 and 27 GPa. In addition to that, the samples without DBs have higher porosity, which, considering that the pores present less resistance than the mineral matrix, contributes to a lower incompressibility modulus than the samples with DBs

We can infer that both the samples with the presence of DBs and the samples obtained between bands have a behavior that is marked by low Poisson's ratio values ranging from 0.204 to 0.199, respectively (Fig. 9D). However, it is necessary to emphasize that even when these rocks present similar brittle behavior, they have different porosities

5. Discussion

The concept of fault zone employed here differs from the classical standard, where the deformation was described as homogeneously concentrated in the fault core and progressively decreased as it moved away from it. The concept proposed by Faulkner et al.,[25,53] for multiples cores, and Choi et al.,[54] for fault zone across the fault, is the closest to what we observed in our study area. However, these authors propose this pattern of multiple cores for faults, and here we observed the same behavior applied to sub-seismic structures with centimetric off-sets. This pattern occurs in all outcrops with the presence of DBs, vary-

UNCORRECTED PROOF

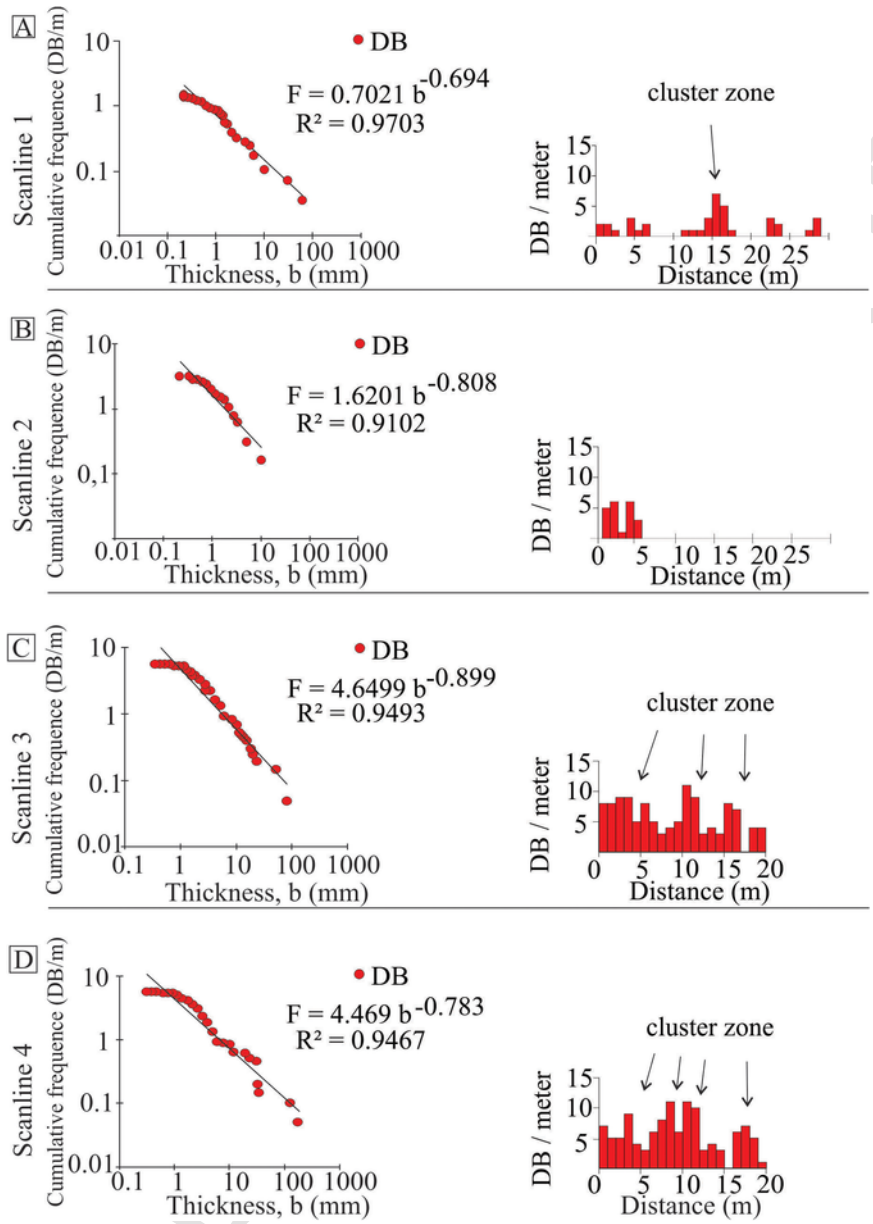

Fig. 7. Scanlines performed in the (A, B) single fault zone and (C, D) complex fault zone. Key: F = frequency of DBs in bands/m; b = Thickness in millimetres.

Table 2
Porosity values acquired through high resolution image analyses.

Architectural element	Porosity (%)
Protolith	7.7
Protolith	18.61
Protolith	5.38
Protolith	9.77
single fault zone	5.27
single fault zone	11.17
single fault zone	10.33
Complex Fault Zone	4.39
Complex Fault Zone	0.2
Complex Fault Zone	1.49
Complex Fault Zone	2.64
Complex Fault Zone	0.95
Complex Fault Zone	1.97
Complex Fault Zone	4.55
Complex Fault Zone	3.29

ing in their number of fault cores and deformation intensity. Complex fault zone present a high number of fault cores and damage zones and single fault zone present lower number of deformation bands, thus lower deformation intensity, showing only one isolated fault core.

Based on field data, UCS and petrophysical analysis, it was possible to individualize and to characterize the different architectural elements and find relationships between them. It is important to state that since the analysed rocks are affected by structures that are capable of changing the petrophysical properties of rocks, the samples are very heterogeneous. However, the samples were individualized accordingly with its deformation intensities. We compared the deformed samples with non-deformed samples to distinguish the deformation intensities. It allowed us to obtain acceptable data.

In the protolith domain, the sedimentary structures, such as cross-stratifications, are well-preserved (Nicchio et al.[32]). Additionally, the protolith presents no deformation bands. Microscopically, the main characteristics are the predominance of punctual grain contacts and the

UNCORRECTED PROOF

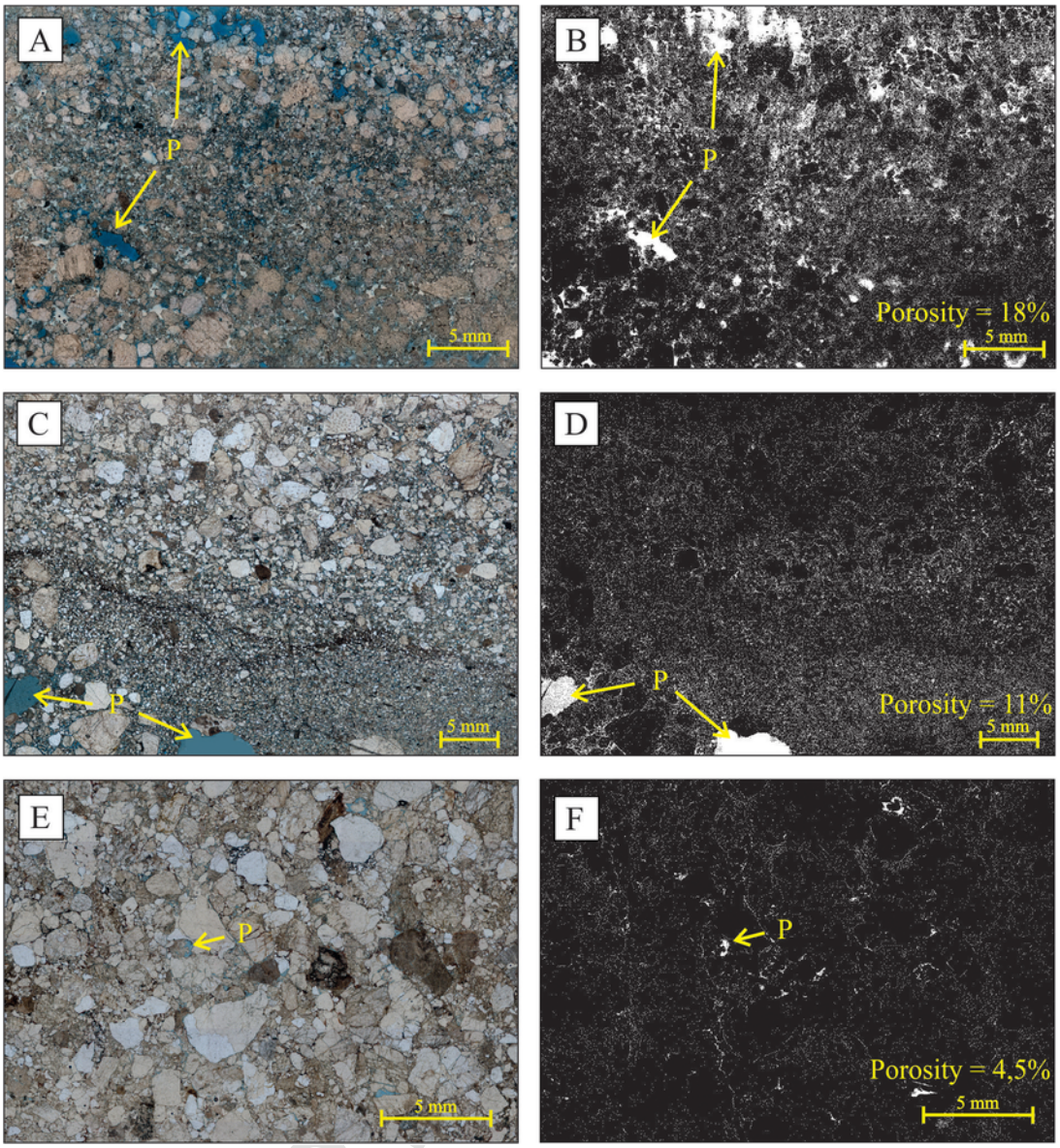

Fig. 8. Photomicrography of the three structural domains and their related images processed by the Imago software: (A, B) protolith, (C, D) single fault zone, and (E, F) complex fault zone. Key: P = Porosity; Pc = Punctual contact; Lc = Long contact;Fr = Fracture formed by compaction;Sc = Sutured contact.

lack of fracturing in grain contacts. Thus suggesting a low compaction degree.

In the single fault zone, a porosity reduction of about 10% occurs compared to the protolith. Porosity reduction of around 10–25% in rocks affected by DBs was observed previously by Mollema and Antonellini,[5] Fossen and Bale[10] and Ballas et al.[55,56] This reduction occurs due to the cataclasis that generates intense grain size reduction, which in turn fill the pores. However, in the single fault zone, the level of cataclasis is low to moderate, allowing some porosity preservation.

The DBs in the single fault zone strikes in two directions, NE-SW and EW, with low occurrence of slip surfaces. The occurrence of slip surfaces is localized and present low frequency, thus suggesting that the exposed deformation bands are not sufficiently well developed to form several slip surfaces (Fossen et al.[4]). Certainly, the increasing strain rate would increase the DBs frequency and would generate DBs in more directions, well-developed clusters and several slip surfaces. The low occurrence of slip-surfaces and clusters is a key factor in the differentiation of the deformation between zones with different levels of deformation, as damage zone and fault core,[27,54] considering that these structures are formed only after high deformation rate accommodated.[4,6]

According to Alikarami et al.[16] mechanical properties vary according to the density of deformation structures. The single fault zone has a moderate number of DBs, and compared with others structural domains this zone has moderates values of UCS too. These moderate values of UCS are response to moderate deformation imposed by the DBs at that location, considering that there was some preservation of the porosity and thus sufficient space to accommodate the deformation. Cataclastic zones occur inside the DBs,[3,26,57,58] with higher rates of deformation and comminution of grain than the zones between DBs. The zones between DBs exhibit lower values of UCS if compared with DBs, which proves a direct relationship between UCS, deformation rates and porosity. Moreover, sandstones affected by DBs exhibit the same behavior of others porous rocks, where the porosity increase leads to a decrease the UCS.[59]

There was a reduction of ~75% in the porosity values in the complex fault zone compared to the protolith. This reduction of porosity is in agreement with what has been described in the literature for cata-

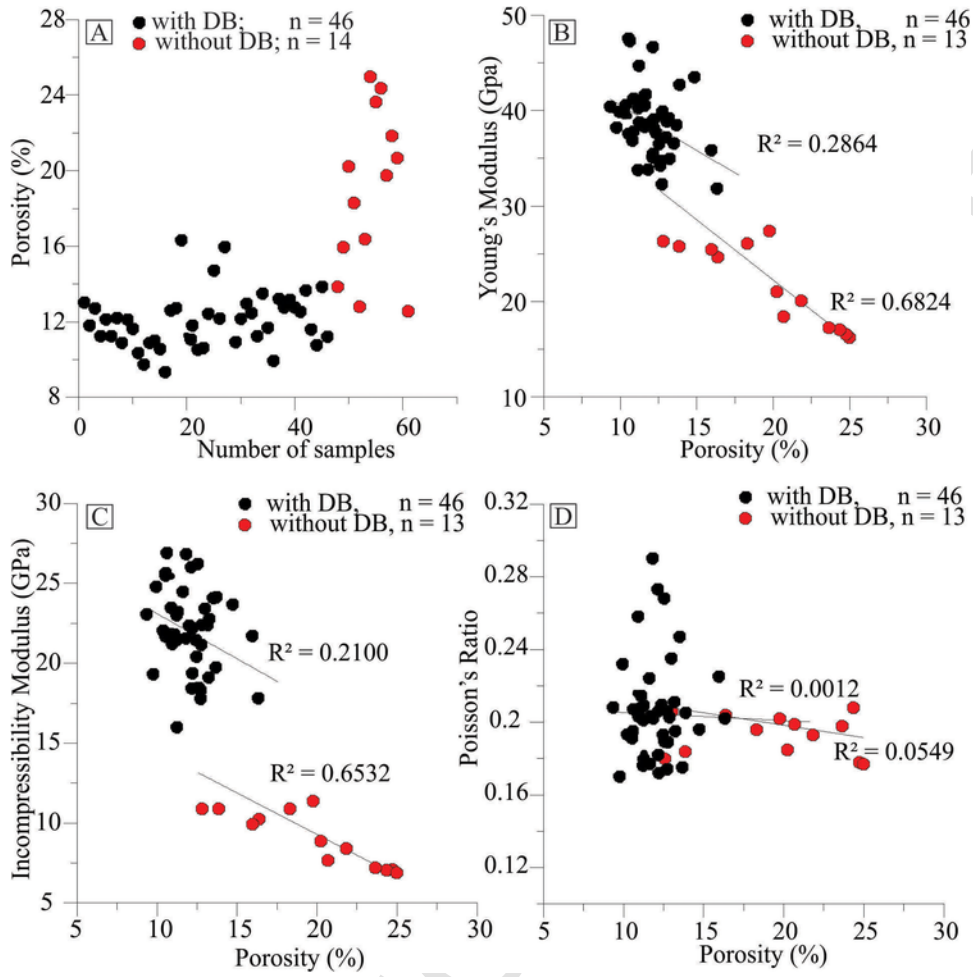

Fig. 9. (A) Porosity *vs.* Number of samples; (B) Young's modulus *vs.* Porosity; (C) Incompressibility modulus *vs.* Porosity; and (D) Poisson's ratio *vs.* Porosity.

clastic bands,[4,9,13,17,60] where some bands present decrease in porosity and permeability of up to six orders of magnitude when compared with the host rock, as seen by Fossen and Bale.[4] In the complex fault zone, the cataclasis was intense enough to reduce the porosity and pore connection (Fig. 3 A, B), which indicates that the DBs acted as fluid flow barrier.

In the complex fault zone, the number of DBs per meter is four times higher than in the single fault zone. The average of DBs thickness ranges from 5.0 to 7.5 mm in the complex fault zone whereas in the single one it ranges from 1.9 m to 4.6 mm. This thus indicate that the complex zone underwent higher deformation rates. This higher deformation rate is also marked by the massive presence of slip surfaces and gouge.

The highest values of UCS are present in the complex fault zone (Fig. 6), for both values within the DB's and between the DBs. As the cataclasis intensity increases within the DBs, the grain size tends to be extremely reduced, allowing the new generated fine grains to be accommodated, filling the remaining pore space. This effect occurs until there is no more pore space to be filled, resulting in an extremely deformed zone, were the compaction is intense, thus affecting the rock by increasing its strength and drastically reducing its porosity. However, it is important to emphasize that this zone of high resistance is not restricted only to the DBs, but also to the zones around it, that is also considered as complex fault zone.

It is important to state that the presence of DBs is related to more intensely deformed zones, thus anisotropic zones. The related faults in this work present low displacement (less than 1,5 m) with the most important ones presenting 1 – 2 m thickness. Thus, the studied faults are considered subseismic structures. The identification and quantification of the petrophysical and geomechanical modifications are useful to support the prediction of the behavior of reservoirs affected by DB. The knowledge of these properties may be applied for fluid flow simulation as oil exploration strategy.

6. Conclusions

The present study analyzes the variation of petrophysical and geomechanical properties in the Rio do Peixe Basin in coarse sandstones across a faults zone composed from the undeformed protolith, single fault zone and complex fault zone, integrating analysis techniques in macro and micro-scale. The results has shown that DBs directly influence petrophysical and geomechanical properties of rock, however these properties are strongly controlled by the structural domain in which the rock are found. We present below the most important results of this study below.

The presence of DBs causes reduction of porosity (Fig. 9 A) and increase of UCS (Fig. 6), as is effective in increasing Young's and incompressibility modules. For both modules, the rock with DBs presents a value of 40% greater than the rock without bands. Considering that the pores have less resistance to deformation than the matrix, it is expected that the areas with DBs, which have a significant reduction in porosity, present higher values of these modules. On the other hand, the Poisson's Ratio values are similar to samples with DB and without DB,

around 0.199–0.204. This value indicates brittle behavior of both the fault core with DBs, and in the areas between bands.

UCS values are higher in DBs than between bands. This increase in resistance is associated with the cataclasis generated by the DBs during it formation. However, the complex fault zone, even at the points between bands, showed values of UCS higher than the rocks found in the single fault zone and protolith. It is concluded that even though DBs generates up to 40% increase in the UCS values, the deformational scenario where the rock is located strongly controls rock resistance.

The complex fault zone presents DBs frequency four times higher than the single fault zone. The complex fault zone also presents bands with higher average thickness and greater clustering of bands in relation to the single fault zone, and the displacement of less than 1 m for the single fault zone and between 1 and 1,5 m displacement for each individual fault zone present in the complex fault zone. These data contribute to the characterization of both architectural elements, considering that a high degree of deformation will produce a greater number of bands, with thicker bands and more clusters.

The porosities calculated from the photomicrographs analysis showed an average value of 10.3% for the undeformed protolith, 8.9% for the single fault zone and 2.4% in the complex fault zone. The fault core present an average porosity value up to 75% smaller than the undeformed protolith, being the presence of DB the cause of this reduction. We conclude that the larger the number of DBs, the lower the porosity values in the architectural elements of the fault zone.

DBs directly influence the compartmentalization and behavior of the geomechanical and hydraulic properties of the sedimentary units. Regardless of whether it is at the fault core or damage zone, the higher the deformation rate, the higher is the UCS values, the lower the porosity values, the greater the number and thickness of bands and the greater the Young and incompressibility modules.

The multi-scale approach of this work, using the upscaling technique to observe the deformation started from a regional scale with the observation of the main brittle structures of the basin, meso scale with geomechanical analysis and collect of structural attributes in outcropping micro scale with petrophysical measurements plug scale and thin sections contributed to the simulation of the fluid flow and estimation of the behavior of the reservoir during its production and depletion.

Uncited reference

61

Acknowledgments

This work was funded by a Petrobras/UFCG project (Multiscale Analysis of the Influence of Deformation Bands in the accumulation and migration of fluids in consolidated reservoir analogues) granted to the Federal University of Campina Grande, Dr. Francisco C. C. Nogueira. The authors wish to thank the Petrobras-Research and Development Center (CENPES) for thin section images. We also thank the Brazilian Oil and gas agency (ANP).

References

1. A. Aydin, Small faults formed as deformation bands in sandstone, Pure Appl Geophys 116 (4–5) (1978) 913–930, https://doi.org/10.1007/BF00876546.
2. A. Aydin, A.M. Johnson, Development of faults as zones of deformation bands and as slip surfaces in sandstone, Pure Appl Geophys 116 (4–5) (1978) 931–942, https://doi.org/10.1007/BF00876547.
3. M.A. Antonellini, A. Aydin, D.D. Pollard, Microstructure of deformation bands in porous sandstones at Arches National Park, Utah, J Struct Geol 16 (7) (1994) 941–959, https://doi.org/10.1016/0191-8141(94)90077-9.
4. H. Fossen, R.A. Schultz, Z.K. Shipton, K. Mair, Deformation bands in sandstone: a review, J Geol Soc Lond 164 (2007) 1–15, https://doi.org/10.1144/0016-76492006-036.
5. P.N. Mollema, M.A. Antonellini, Compaction bands: a structural analog for anti-mode I cracks in aeolian sandstone, Tectonophysics 267 (1–4) (1996) 209–228, https://doi.org/10.1016/S0040-1951(96)00098-4.
6. Z.K. Shipton, P.A. Cowie, Damage zone and slip-surface evolution over micro-m to km scales in high-porosity Navajo sandstone, Utah, J Struct Geol 23 (12) (2001) 1825–1844, https://doi.org/10.1016/S0191-8141(01)00035-9.
7. H.E. Edwards A.D. Becker J.A. Howell Compartmentalisation of an eolian sandstone by structural heterogeneities: Permo-Triassic Hopeman Sandstone, Moray Firth, Scotland Geol Soc London 1993339–365 [Special Pu]
8. K. Mair, I. Main, S. Elphick, Sequential growth of deformation bands in the laboratory, J Struct Geol 22 (1) (2000) 25–42, https://doi.org/10.1016/S0191-8141(99)00124-8.
9. G. Ballas, R. Soliva, A. Benedicto, J.P. Sizun, Control of tectonic setting and large-scale faults on the basin-scale distribution of deformation bands in porous sandstone (Provence, France), Mar Pet Geol 55 (2014) 142–159, https://doi.org/10.1016/j.marpetgeo.2013.12.020.
10. H. Fossen, A. Bale, Deformation bands and their influence on fluid flow, Am Assoc Pet Geol Bull 91 (12) (2007) 1685–1700, https://doi.org/10.1306/07300706146.
11. R. Soliva, G. Ballas, H. Fossen, S. Philit, Tectonic regime controls clustering of deformation bands in porous sandstone, Geology 44 (6) (2016) 423–426, https://doi.org/10.1130/G37585.1.
12. J. Parnell, G.R. Watt, D. Middleton, J. Kelly, M. Baron, Deformation band control on hydrocarbon migration, J Sediment Res 74 (4) (2004) 552–560, https://doi.org/10.1306/121703740552.
13. A. Torabi, Cataclastic bands in immature and poorly lithified sandstone, examples from Corsica, France, Tectonophysics 630 (C) (2014) 91–102, https://doi.org/10.1016/j.tecto.2014.05.014.
14. C.A.J. Wibberley, J.P. Petit, T. Rives, The mechanics of fault distribution and localization in high-porosity sands, Provence, France Geol Soc London 200719–46, https://doi.org/10.1144/SP289.3[Spec Publ].
15. J.F. Bauer, S. Meier, S.L. Philipp, Architecture, fracture system, mechanical properties and permeability structure of a fault zone in Lower Triassic sandstone, Upper Rhine Graben, Tectonophysics 647 (2015) 132–145, https://doi.org/10.1016/j.tecto.2015.02.014.
16. R. Alikarami, A. Torabi, D. Kolyukhin, E. Skurtveit, Geostatistical relationships between mechanical and petrophysical properties of deformed sandstone, Int J Rock Mech Min Sci 63 (2013) 27–38, https://doi.org/10.1016/j.ijrmms.2013.06.002.
17. F. Balsamo, F. Storti, F. Salvini, A.T. Silva, C.C. Lima, Structural and petrophysical evolution of extensional fault zones in low-porosity, poorly lithified sandstones of the Barreiras Formation, NE Brazil, J Struct Geol 32 (11) (2010) 1806–1826, https://doi.org/10.1016/j.jsg.2009.10.010.
18. E. Ravier, M. Guiraud, A. Guillien, E. Vennin, J.F. Buoncristiani, E. Portier, Micro- to macro-scale internal structures, diagenesis and petrophysical evolution of injectite networks in the Vocontian Basin (France): implications for fluid flow, Mar Pet Geol 64 (2015) 125–151, https://doi.org/10.1016/j.marpetgeo.2015.02.040.
19. A. Rotevatn, E. Thorsheim, E. Bastesen, H.S.S. Fossmark, A. Torabi, G. Sælen, Sequential growth of deformation bands in carbonate grainstones in the hangingwall of an active growth fault: implications for deformation mechanisms in different tectonic regimes, J Struct Geol 90 (2016) 27–47, https://doi.org/10.1016/j.jsg.2016.07.003.
20. H. Jourde, E.A. Flodin, A. Aydin, L.J. Durlofsky, X.H. Wen, Computing permeability of fault zones in eolian sandstone from outcrop measurements, Am Assoc Pet Geol Bull 86 (7) (2002) 1187–1200, https://doi.org/10.1306/61EEDC4C-173E-11D7-8645000102C1865D.
21. I. Ylmaz, H. Sendir, Correlation of Schmidt hardness with unconfined compressive strength and young's modulus in gypsum from Sivas (Turkey), Eng Geol 66 (3–4) (2002) 211–219, https://doi.org/10.1016/S0013-7952(02)00041-8.
22. A. Torabi, H. Fossen, Spatial variation of microstructure and petrophysical properties along deformation bands in reservoir sandstones, Am Assoc Pet Geol Bull 93 (7) (2009) 919–938, https://doi.org/10.1306/03270908161.
23. S. Schueller, A. Braathen, H. Fossen, J. Tveranger, Spatial distribution of deformation bands in damage zones of extensional faults in porous sandstones: statistical analysis of field data, J Struct Geol 52 (1) (2013) 148–162, https://doi.org/10.1016/j.jsg.2013.03.013.
24. F.M. Chester, J.M. Logan, Composite planar fabric of gouge from the Punchbowl Fault, California, J Struct Geol 9 (5–6) (1987) https://doi.org/10.1016/0191-8141(87)90147-7.
25. D.R. Faulkner, C.A.L. Jackson, R.J. Lunn, et al., A review of recent developments concerning the structure, mechanics and fluid flow properties of fault zones, J Struct Geol 32 (11) (2010) 1557–1575, https://doi.org/10.1016/j.jsg.2010.06.009.
26. A. Torabi, H. Fossen, A. Braathen, Insight into petrophysical properties of deformed sandstone reservoirs, Am Assoc Pet Geol Bull 97 (4) (2013) 619–637, https://doi.org/10.1306/10031212040.
27. Z.K. Shipton, P.A. Cowie, A conceptual model for the origin of fault damage zone structures in high-porosity sandstone, J Struct Geol 25 (3) (2003) 333–344, https://doi.org/10.1016/S0191-8141(02)00037-8.
28. C.A.J. Wibberley, G. Yielding, G. Di Toro, et al., Recent advances in the understanding of fault zone internal structure: a review Geol Soc London 20085–33, https://doi.org/10.1144/SP299.2[Spec Publ].
29. J.B.L. Françolin, P.R. Cobbold, P. Szatmari, Faulting in the Early Cretaceous Rio do Peixe basin (NE Brazil) and its significance for the opening of the Atlantic, J Struct Geol 16 (5) (1994) 647–661, https://doi.org/10.1016/0191-8141(94)90116-3.
30. F.C.C. Nogueira, F.O. Marques, F.H.R. Bezerra, D.L. de Castro, R.A. Fuck, Cretaceous intracontinental rifting and post-rift inversion in NE Brazil: Insights from the Rio do Peixe Basin, Tectonophysics 644 (2015) 92–107, https://doi.org/10.1016/j.tecto.2014.12.016.
31. J. Sénant, M. Popoff, Early Cretaceous extension in northeast Brazil related to the South Atlantic opening, Tectonophysics 198 (1) (1991) 35–46, https://doi.org/10.

UNCORRECTED PROOF

32. M.A. Nicchio, F.C.C. Nogueira, F. Balsamo, et al., Development of cataclastic foliation in deformation bands in feldspar-rich conglomerates of the Rio do Peixe Basin, NE Brazil, J Struct Geol 107 (2018) 132–141, https://doi.org/10.1016/j.jsg.2017.12.013.
33. R.E.B. Araujo, F.H.R. Bezerra, F.C.C. Nogueira, et al., Basement control on fault formation and deformation band damage zone evolution in the Rio do Peixe Basin, Brazil, Tectonophysics 745 (2018) 117–131, https://doi.org/10.1016/j.tecto.2018.08.011.
34. O.P.G. Braun Geologia Da Bacia Do Rio Do Peixe, Nordeste Do Brasil, Relatório de Prospecção 1969
35. D.L. de Castro, D.C. de Oliveira, R.M. Gomes Castelo Branco, On the tectonics of the Neocomian Rio do Peixe Rift Basin, NE Brazil: Lessons from gravity, magnetics, and radiometric data, J South Am Earth Sci 24 (2–4) (2007) 184–202, https://doi.org/10.1016/j.jsames.2007.04.001.
36. W.S. Dershowitz, H.H. Herda, Interpretation of fracture spacing and intensity, US Symp Rock Mech (1992) 757–766.
37. R. Marrett, O.J. Ortega, C.M. Kelsey, Extent of power-law scaling for natural fractures in rock, Geology 27 (9) (1999) 799–802, https://doi.org/10.1130/0091-7613(1999)027<0799:EOPLSF>2.3.CO.
38. O.J. Ortega, R.A. Marrett, S.E. Laubach, A scale-independent approach to fracture intensity and average spacing measurement, Am Assoc Pet Geol Bull 90 (2) (2006) 193–208, https://doi.org/10.1306/08250505059.
39. Miranda TS, Barbosa JA, Gale JFW. et al. Natural Fracture Characterization in Aptian Carbonates, Araripe Basin, NE Brazil. In: Proceedings of the 76th EAGE Conference & Exphibition. Amsterdam, The Netherlands; 2014.
40. D.J. Sanderson, C.W. Nixon, The use of topology in fracture network characterization, J Struct Geol 72 (2015) 55–66, https://doi.org/10.1016/j.jsg.2015.01.005.
41. A. Aydin, ISRM Suggested method for determination of the Schmidt hammer rebound hardness: revised version, Int J Rock Mech Min Sci 46 (3) (2009) 627–634, https://doi.org/10.1016/j.ijrmms.2008.01.020.
42. A. Aydin, A.M. Johnson, Analysis of faulting in porous sandstones, J Struct Geol 5 (1) (1983) 19–31, https://doi.org/10.1016/0191-8141(83)90004-4.
43. ASTM Standard test method for determination of rock hardness by rebound hammer method ASTM International West Conshohocken 2001
44. P. Baud, T. fong Wong, W. Zhu, Effects of porosity and crack density on the compressive strength of rocks, Int J Rock Mech Min Sci 67 (2014) 202–211, https://doi.org/10.1016/j.ijrmms.2013.08.031.
45. R. Marrett, Aggregate properties of fracture populations, J Struct Geol 18 (2–3) (1996) 169–178, https://doi.org/10.1016/S0191-8141(96)80042-3.
46. J.F.W. Gale, L.A. Gomez, Late opening-mode fractures in karst-brecciated dolostones of the Lower Ordovician Ellenburger Group, west Texas: recognition, characterization, and implications for fluid flow, Am Assoc Pet Geol Bull 91 (7) (2007) 1005–1023, https://doi.org/10.1306/03130706066.
47. R.D. Terzaghi, Sources of Error in Joint Surveys, Géotechnique 15 (3) (1965) 287–304, https://doi.org/10.1680/geot.1965.15.3.287.
48. V. Guerriero, A. Iannace, S. Mazzoli, M. Parente, S. Vitale, M. Giorgioni, Quantifying uncertainties in multi-scale studies of fractured reservoir analogues: implemented statistical analysis of scan line data from carbonate rocks, J Struct Geol 32 (9) (2010) 1271–1278, https://doi.org/10.1016/j.jsg.2009.04.016.
49. J.N. Hooker, S.E. Laubach, R. Marrett, Fracture-aperture sizedfrequency, spatial distribution, and growth processes in strata-bounded and non-strata-bounded fractures, cambrian mesón group, NW argentina, J Struct Geol 54 (2013) 54–71, https://doi.org/10.1016/j.jsg.2013.06.011.
50. J.G. Solum, J.P. Brandenburg, S.J. Naruk, O.V. Kostenko, S.J. Wilkins, R.A. Schultz, Characterization of deformation bands associated with normal and reverse stress states in the Navajo Sandstone, Utah, Am Assoc Pet Geol Bull 94 (9) (2010) 1453–1475, https://doi.org/10.1306/01051009137.
51. P.A. Gillespie, J.J. Walsh, J. Watterson, C.G. Bonson, T. Manzocchi, Scaling relationships of joint and vein arrays from The Burren, Co. Clare, Ireland, J Struct Geol 23 (2–3) (2001) 183–201, https://doi.org/10.1016/S0191-8141(00)00090-0.
52. D. Kolyukhin, A. Torabi, Statistical analysis of the relationships between faults attributes, J Geophys Res Solid Earth 117 (5) (2012) 1–14, https://doi.org/10.1029/2011JB008880.
53. D.R. Faulkner, A.C. Lewis, E.H. Rutter, On the internal structure and mechanics of large strike-slip fault zones: field observations of the Carboneras fault in southeastern Spain, Tectonophysics 367 (3–4) (2003) 235–251, https://doi.org/10.1016/S0040-1951(03)00134-3.
54. J.H. Choi, P. Edwards, K. Ko, Y.S. Kim, Definition and classification of fault damage zones: a review and a new methodological approach, Earth-Sci Rev 152 (2016) 70–87, https://doi.org/10.1016/j.earscirev.2015.11.006.
55. G. Ballas, R. Soliva, J.P. Sizun, H. Fossen, A. Benedicto, E. Skurtveit, Shear-enhanced compaction bands formed at shallow burial conditions; implications for fluid flow (Provence, France), J Struct Geol 47 (2013) 3–15, https://doi.org/10.1016/j.jsg.2012.11.008.
56. G. Ballas, H. Fossen, R. Soliva, Factors controlling permeability of cataclastic deformation bands and faults in porous sandstone reservoirs, J Struct Geol 76 (July) (2015) 1–21, https://doi.org/10.1016/j.jsg.2015.03.013.
57. H. Fossen, Deformation bands formed during soft-sediment deformation: observations from SE Utah, Mar Pet Geol 27 (1) (2010) 215–222, https://doi.org/10.1016/j.marpetgeo.2009.06.005.
58. G. Ballas, H. Fossen, R. Soliva, Factors controlling permeability of cataclastic deformation bands and faults in porous sandstone reservoirs, J Struct Geol 76 (2015) 1–21, https://doi.org/10.1016/j.jsg.2015.03.013.
59. V. Palchik, Influence of porosity and elastic modulus on uniaxial compressive strength in soft brittle porous sandstones, Rock Mech Rock Eng 32 (4) (1999) 303–309, https://doi.org/10.1007/s006030050050.
60. M.C.N. Rodrigues, L. de, B. Trzaskos, A.P. Lopes, Influence of deformation bands on sandstone porosity: a case study using three-dimensional microtomography, J Struct Geol 72 (2015) 96–110, https://doi.org/10.1016/j.jsg.2015.01.003.
61. V.C. Medeiros, C.A. Amaral, Rocha DEGA, R.B. Santos, Programa Geologia do Brasil - PGB. Sousa. Folha SB.24-Z-A. Estados da Paraíba, Rio Grande do Norte e Ceará. Mapa Geológico CPRM Recife 200524.

UNCORRECTED PROOF